

MODELING POLYMER MELT FLOW USING THE PARTICLE FINITE ELEMENT METHOD

Kathryn M. Butler¹, Eugenio Oñate², Sergio R. Idelsohn², and Riccardo Rossi²

¹National Institute of Standards and Technology, USA

²International Center for Numerical Methods in Engineering, Spain

ABSTRACT

A new particle-based approach is applied to the modeling of the melt flow behavior of thermoplastics. The Particle Finite Element Method (PFEM) combines convection of particles by the flow field with a finite element solution of the equations of motion and energy, in a fully Lagrangian formulation that tracks large changes in shape and topology. The potential of this method to model thermoplastic melt flow is tested with a series of computational problems based on flow from an upright rectangular sample heated on one face. The quasi-steady flow rate under three levels of heat flux is about 25 % higher than experimental results, in line with previous modeling results. The addition of gasification to the PFEM model provides good agreement with a 1D analytical model when the gasification layer is well-resolved. A model that includes dripping of the sample onto a catch surface below conserves mass within ± 5 %.

INTRODUCTION

Thermoplastic objects, including mattresses, upholstered furniture, and molded objects such as electronic housings and automobile parts, respond to fire by melting and dripping onto the surface below. The flow of material affects heat and mass transport within the object, and the accumulating melt pool below the object may extend the flaming zone and increase the overall rate of heat release.^{1,2} If the fire from the object and the pool fire interact, the intensity of the fire is enhanced even further. The spread rate of the melt pool and its burning behavior (including whether it is even able to sustain ignition) are affected by the flooring material as well as by the properties of the melt.³ A computer model that successfully predicts flame spread for these objects would provide a powerful tool for improving the flammability of materials. This is an exceptionally complex problem, involving fluid flow, heat transfer, material degradation, flame chemistry, surface tension, and complex material properties. In addition, the drastic changes in shape pose a severe challenge to traditional modeling methods. Attempts to model melt flow of polymeric material in fire using the volume of fluid (VOF) method⁴ have encountered difficulties with numerical instabilities and excessive runtimes.

Over the past decade, new numerical methods have been developed to solve problems involving large deformations of the free surface, such as high speed impact of solids, breaking waves, and granular flow.⁵ In these methods, the governing equations for both fluids and solids are written using a Lagrangian description, which follows the motion of individual particles in the flow. This approach eliminates the convective term in the equations and provides many advantages in computational efficiency. In the Particle Finite Element Method (PFEM),⁶ the particles represent the nodes of a finite element mesh. The particles move freely according to the velocity field, transporting their momentum and physical properties. A robust and efficient remeshing algorithm connects the nodes into a finite element grid for solution of the state variables in the new configuration. The PFEM has been used to solve a variety of free surface, fluid-structure interaction, and multiphase problems, including dam bursting,⁶ ship hydrodynamics,⁷ and metal casting.⁸

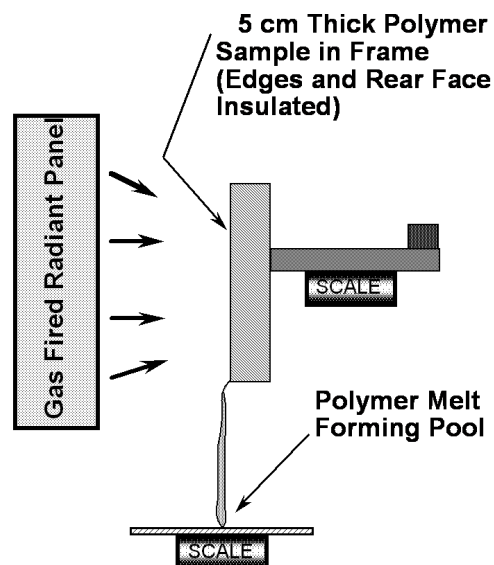
This application of the PFEM is in support of a combined experimental and modeling effort at the National Institute of Standards and Technology (NIST) to clarify the role of the properties of

thermoplastics in their burning behavior, including the effects of flow. The numerical model simulates an experiment in which a slab of polymeric material is mounted vertically and exposed to uniform radiant heating on one face. Degradation of the polymer decreases its viscosity by several orders of magnitude and produces fuel gases. Polymer melt is captured by a pan below the sample. The potential of the PFEM for modeling melt flow of thermoplastic objects in fire was first demonstrated with a two-dimensional solution for flow from the upright slab exposed to heat, with viscosity represented as a simple function of temperature. The solution was obtained on a desktop workstation with a run-time under a day. Subsequently, gasification and a pan for capturing the melt were added. Finally, the step to a three-dimensional solution is demonstrated. Comparisons to experimental results are presented.

MELT FLOW PROBLEM

The modeling effort simulates the behavior from a set of experiments carried out over the past few years by Ohlemiller et al. at NIST.^{4,9} A schematic of the apparatus used in the experiments is shown in Figure 1. A rectangular polymeric sample of dimensions 10 cm high by 10 cm wide by 5 cm thick is mounted upright and exposed to uniform heating on one face from a radiant heater placed on its side. The sample is insulated on its lateral and rear faces. The melt flows down the heated face of the sample and drips onto a surface below. A load cell monitors the mass of polymer remaining in the sample, and a laboratory balance measures the mass of polymer falling onto the catch surface. More details of the experimental setup are given in previous papers.^{4,9}

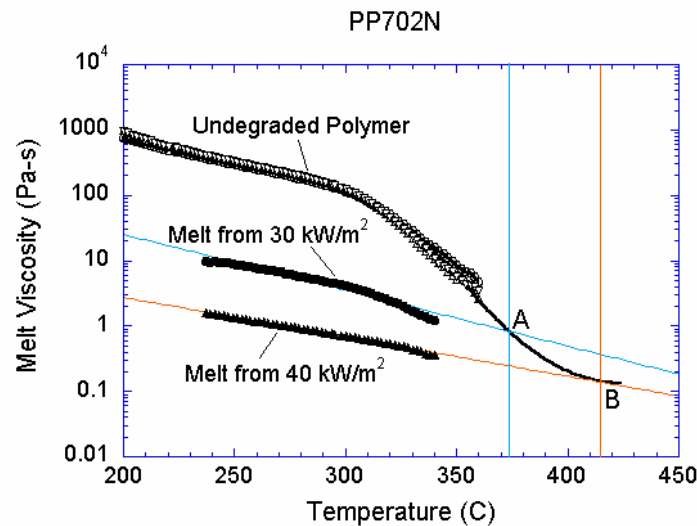
Figure 1. Polymer melt apparatus.



Viscosity is a key determinant of the melting behavior of thermoplastics. A high temperature both increases the mobility of the polymer chains and breaks chemical bonds to create smaller fragments; thus viscosity is a function of both molecular weight and temperature. To avoid calculation of the molecular weight distribution of the polymeric melt, which would greatly increase the complexity of the model, a simple relationship between viscosity and temperature was sought.⁴ A rheometer can measure viscosity as a function of temperature, but only up to the temperature at which the polymer begins to bubble. To carry the curve beyond this point, the rheometer was also used to characterize samples of the melt generated by two different heat flux levels. These melt samples are assumed to have been generated at the surface temperature of the melt as it flows down the heated face, a quantity that is measured during the experiment. This assumption neglects the effects of residence time at a given temperature on molecular weight, but tests found that doubling the residence time does not affect the melt viscosity. Figure 2 shows all three curves of viscosity vs. temperature for the

polypropylene type PP702N, a low viscosity commercial injection molding resin formulation. The relationship used in the model, as shown by the black line, connects the curve for the undegraded polymer to points A and B extrapolated from the viscosity curve for each melt sample to the temperature at which the sample was formed. The result is an empirical viscosity-temperature curve that implicitly accounts for molecular weight changes.

Figure 2. Viscosity vs. temperature for PP702N polypropylene in its initial undegraded form and after exposure to 30 kW/m² and 40 kW/m² heat fluxes. The black curve follows the extrapolation of viscosity to high temperatures.



For the upright object to act as a solid at room temperature over the duration of the experiment, the viscosity at room temperature is set at 10⁶ Pa-s. Linear interpolation between 25 °C and 200 °C maintains the solidity of the sample at low temperatures. At temperatures above 415 °C, the viscosity is set to the value at point B.

Kinetic parameters for an Arrhenius expression for gasification were obtained from thermogravimetric analysis (TGA). Density, thermal conductivity, and specific heat are assigned constant values in the model.

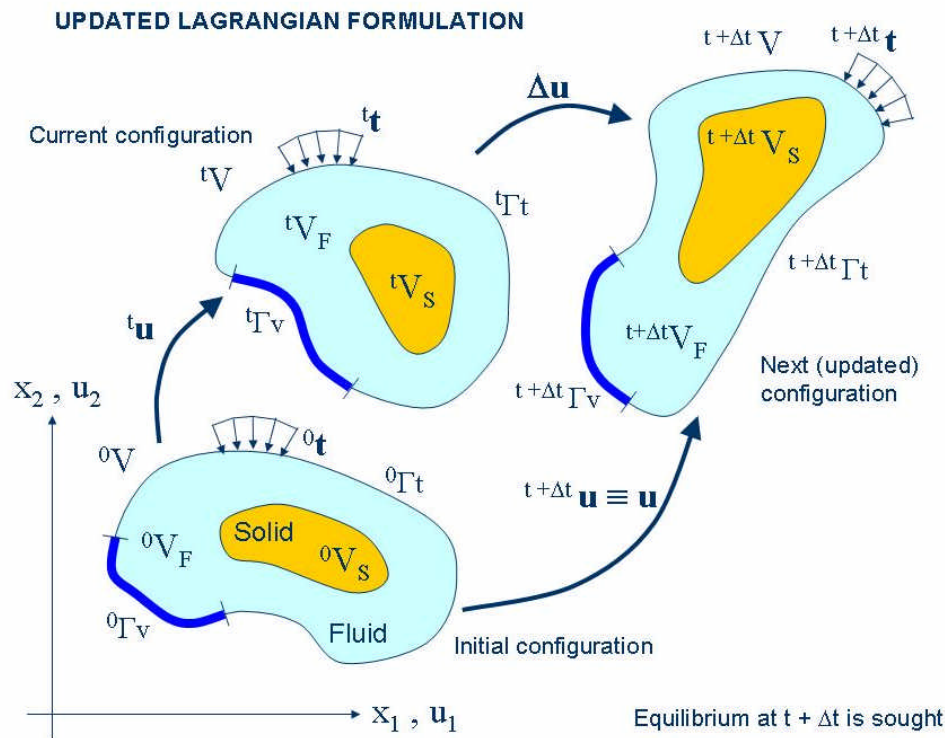
PARTICLE FINITE ELEMENT METHOD

For this computational approach, a domain containing both fluid and solid subdomains is considered. The moving fluid particles interact with the solid boundaries thereby inducing the deformation of the solid which in turn affects the flow motion. The problem is then fully coupled.

In the PFEM both the fluid and the solid domains are modeled using an *updated Lagrangian formulation*. That is, all variables in the fluid and solid domains are assumed to be known in the *current configuration* at time t . The new set of variables in both domains is sought in the *next or updated configuration* at time $t + \Delta t$ (Figure 3). The finite element method (FEM) is used to solve the continuum equations in both domains. Hence a mesh discretizing these domains must be generated in order to solve the governing equations for both the fluid and solid problems in the standard FEM fashion. To do this, the nodes discretizing the fluid and solid domains are treated as *material particles* whose motion is tracked during the transient solution. This is useful to model the separation of fluid particles from the main fluid domain in a splashing wave, or soil particles in a bed erosion problem, and to follow their subsequent motion as individual particles with a known density, an initial acceleration and velocity, and subject to gravity forces. The mass of a given domain is obtained by integrating the density at the different material points over the domain.

The quality of the numerical solution depends on the discretization chosen as in the standard FEM. Adaptive mesh refinement techniques can be used to improve the solution in zones where large motions of the fluid or the structure occur.

Figure 3. Updated Lagrangian description for a continuum containing a fluid and a solid domain.



Basic steps of the PFEM

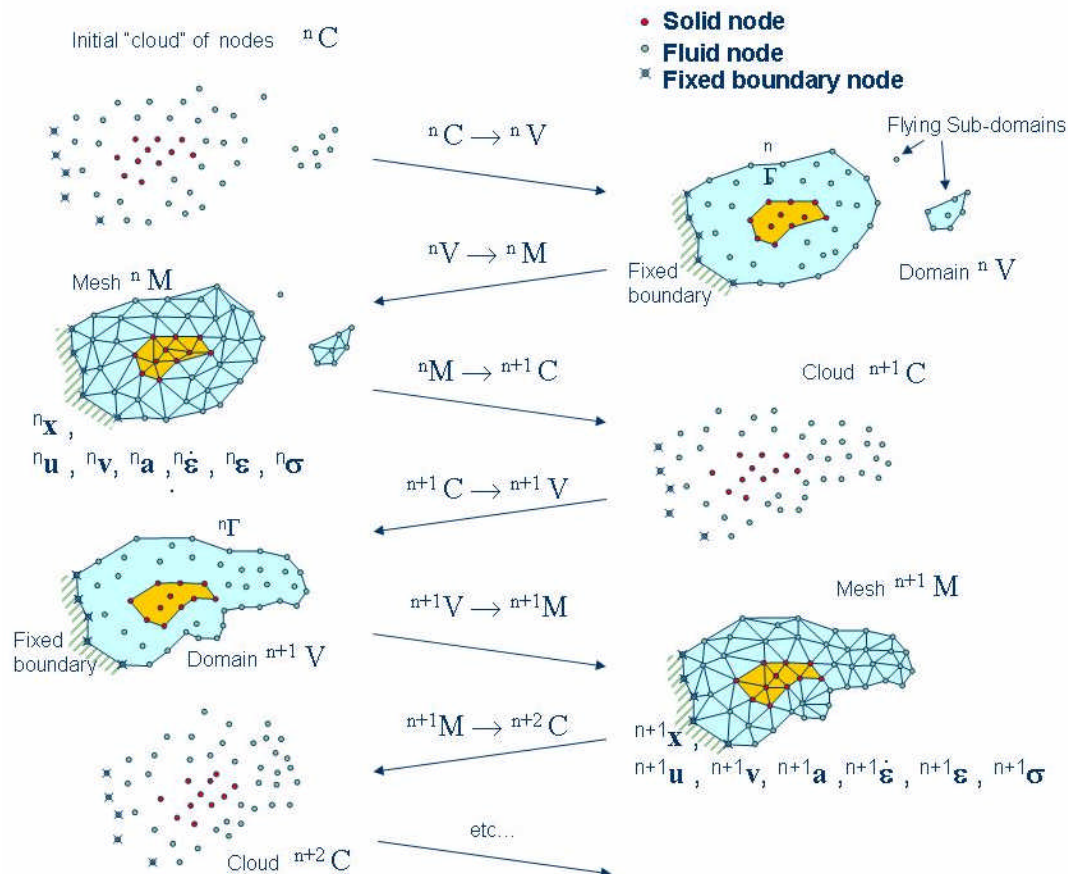
For clarity the *collection or cloud of nodes* pertaining to the fluid and solid domains will be defined as (C), the *volume* defining the analysis domain for the fluid and the solid as (V), and the *mesh* discretizing both domains as (M).

A typical solution with the PFEM involves the following steps.

1. The starting point at each time step is the cloud of points in the fluid and solid domains. For instance, ${}^n C$ denotes the cloud at time $t = t_n$ (Figure 4).
2. Identify the boundaries for both the fluid and solid domains defining the analysis domain ${}^n V$ in the fluid and the solid. This is an essential step as some boundaries (such as the free surface in fluids) may be severely distorted during the solution process including separation and re-entering of nodes. The Alpha-Shape method¹⁰ is used for the boundary definition.
3. Discretize the fluid and solid domains with a finite element mesh ${}^n M$. In this work an innovative mesh generation scheme based on the extended Delaunay tessellation has been used.^{6,7,11}
4. Solve the coupled Lagrangian equations of motion for the fluid and the solid domains. Compute the relevant state variables in both domains at the next (updated) configuration for $t + \Delta t$: velocities, pressure and viscous stresses in the fluid and displacements, stresses and strains in the solid.

5. Move the mesh nodes to a new position ${}^{n+1}C$ where $n+1$ denotes the time $t_n + \Delta t$, in terms of the time increment size. This step is typically a consequence of the solution process of step 4.
6. Go back to step 1 and repeat the solution process for the next time step to obtain ${}^{n+2}C$. The process is shown in Figure 4.

Figure 4. Sequence of steps to update a “cloud” of nodes from time n ($t = t_n$) to time $n+2$ ($t = t_n + 2\Delta t$).



RESULTS

The ability of the PFEM to model thermoplastic melt flow has been tested by modeling the flow of material out of the heated sample and comparing the results to experiment, checking the mass loss rate of gasification against a 1D model, and testing the conservation of mass when a catch pan is added below the sample to capture the dripping melt. The results of the model are visualized using the GiD pre- and post-processor.*

Flow from heated sample

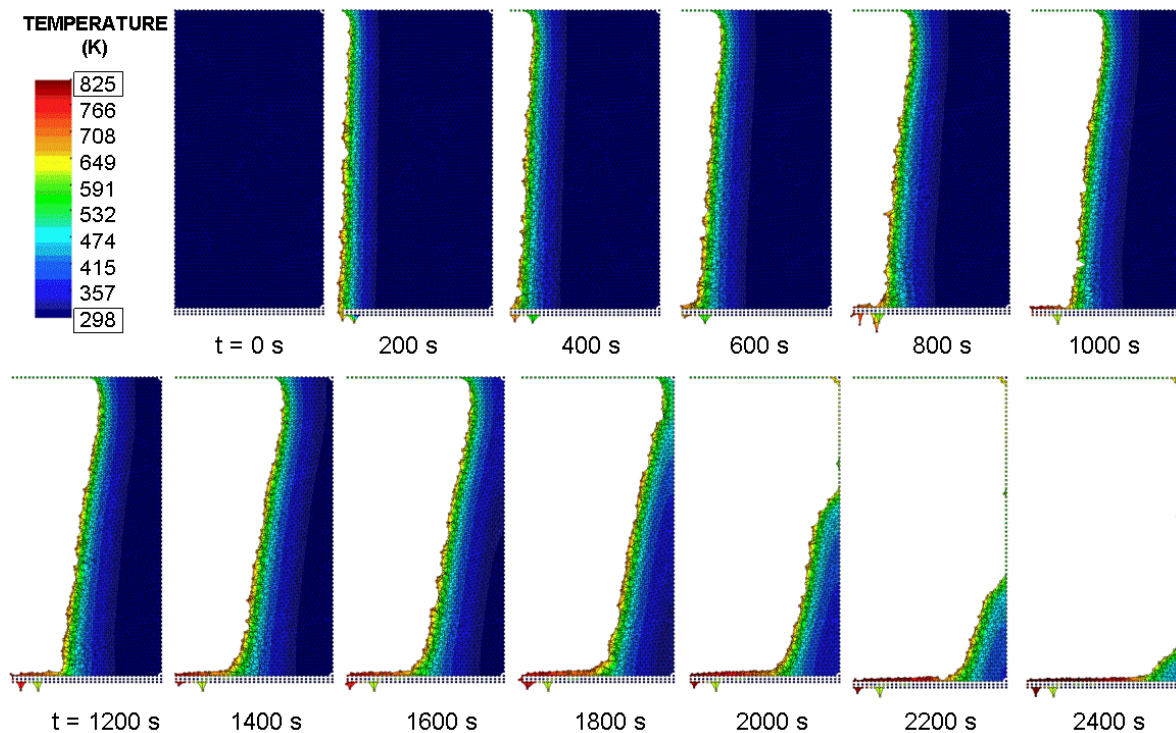
The starting point for modeling this set of experiments is a 2D upright rectangle 10 cm tall and 5 cm thick, with the left face designated as a free surface and upper, lower, and right (or back)

* Certain trade names and company products are mentioned in the text in order to specify adequately the equipment used. In no case does such identification imply recommendation or endorsement by the National Institute of Standards and Technology, nor does it imply that the products are necessarily the best available for the purpose.

faces satisfying no-slip and adiabatic boundary conditions. Gravity is directed downwards. The free surface is exposed to a steady heat flux, and the boundary condition for the heated surface includes convective and radiative losses. The spatial resolution is initially uniform throughout. An initial spacing of 2.0 mm between particles results in a finite element model of 1537 nodes and 2818 elements, while a spacing of 1.4 mm results in 3098 nodes and 5832 elements. Since no particles are added during the course of the run, the size of the finite element grid decreases with time.

A time sequence of the shape and temperature of the heated sample is shown in Figure 5. The heat flux for this problem is 30 kW/m^2 , and the initial spacing is 1.4 mm.

Figure 5. Time sequence showing flow from heated polymer sample.



As the material flows out of the sample near the lower left corner, the free surface develops a slope from lower left to upper right that moves to the right as the polymer melt flows out of the sample. A curvature in the free surface near the top face reflects the no-slip boundary conditions there. Before particles flow out of the problem, they populate a thin flow region along the lower face with high temperature and therefore low viscosity. As they fall from the sample, a small number of particles are recaptured and form new elements under the lower face of the object. Two rows of fixed nodes prevent these anomalous elements from heating the material above the lower face.

Cases were run for three heat fluxes and two spatial resolutions. Figure 6 shows the development of the sample mass with time. During initial heating, the viscosity remains too high for the particles to undergo significant movement, and the mass is steady. After flow begins, the sample enters a long quasi-steady period, during which the mass decreases linearly with time and therefore the mass loss rate is constant with time, as the free surface of the melt flow moves back. When the free surface reaches the top of the back wall, at about $t = 1800 \text{ s}$ for the sequence at 30 kW/m^2 in Figure 5, the mass loss rate speeds up. As the top point of contact with the back face loses height, the mass loss rate slows again, until the material has completely flowed out.

Figure 6. Mass as a function of time for sample exposed to heat fluxes of 20, 30, and 40 kW/m², with two spatial resolutions for each heat flux level.

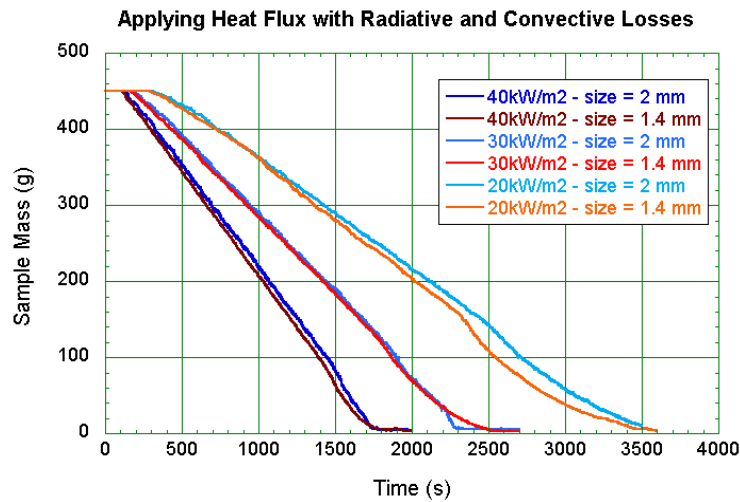
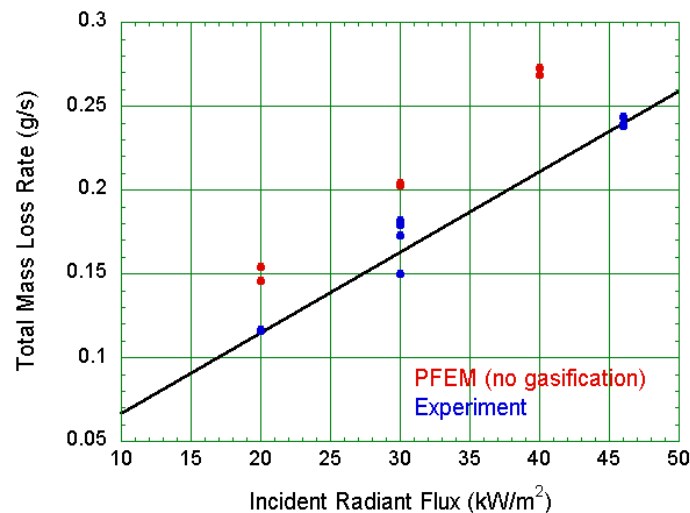


Figure 7 compares the mass loss rate of the quasi-steady period with that obtained from experiments at three levels of heat flux. The mass loss rate follows the same trend, with values about 25 % higher than the experimental data. Note that this model does not yet include gasification or in-depth absorption of radiation, both of which are expected to increase the mass loss rate. This discrepancy will eventually require further study.

Figure 7. Comparison of PFEM model to experiments for mass loss rate as a function of incident radiant flux .

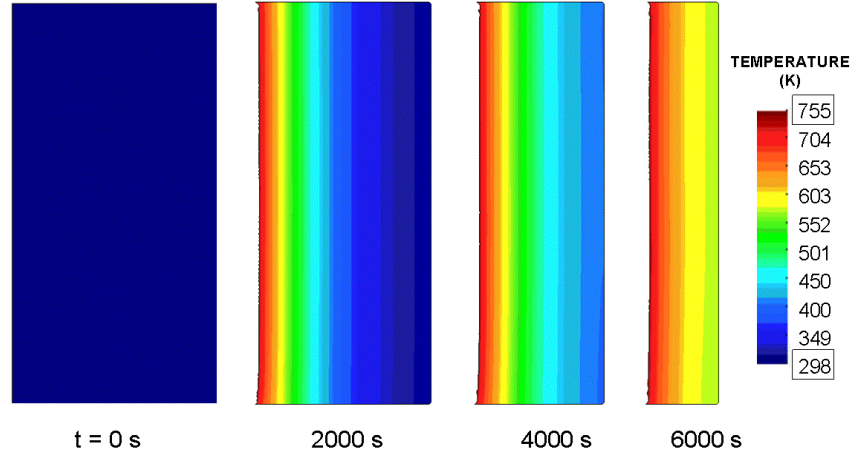


Gasification

Gasification is represented by Arrhenius expressions in both mass and energy equations. This capability was added to the PFEM by including the nonlinear energy loss term in the energy equation and replacing the incompressibility constraint $\nabla \cdot u = 0$ with the temperature-dependent mass loss term $\nabla \cdot u = B \exp(-E/RT)$. In this equation, B is the pre-exponential factor, E is activation energy, and R is the gas constant. To test the implementation, gravity is set to 0 and flow is eliminated. The sensitivity to resolution is tested using three cases, with initial spacing between particles equal to 1.4 mm with 3098 nodes and 5832 elements, 1.0 mm with 5958 nodes and 11410 elements, and 0.5 mm with 23396 nodes and 45786 elements.

Figure 8 shows a time sequence of the gasifying sample with an initial spacing of 0.5 mm. The free surface is flat throughout gasification, except for some small oscillations near the no-slip walls at top and bottom.

Figure 8. Time sequence of PFEM model undergoing gasification without melt flow.



The accuracy of the PFEM model was checked by comparison to a 1D model of gasification that solves the identical problem. The 1D model solves the energy equation for a gasifying slab of material of thickness L heated at incident heat flux q_0 at $z = L$:

$$\rho c_p \left(\frac{\partial T}{\partial t} + W \frac{\partial T}{\partial z} \right) + H_v \frac{dm}{dt} = k \frac{\partial^2 T}{\partial z^2} \quad , \quad [1]$$

where T is temperature, ρ is density, c_p is specific heat, k is thermal conductivity, H_v is the heat of vaporization, and mass loss rate is given by the Arrhenius expression:

$$\frac{dm}{dt} = \rho B e^{-E/RT} \quad . \quad [2]$$

The velocity W at any position z within the slab is

$$W(z, t) = - \int_0^z \frac{(dm/dt)}{\rho} dz \quad , \quad [3]$$

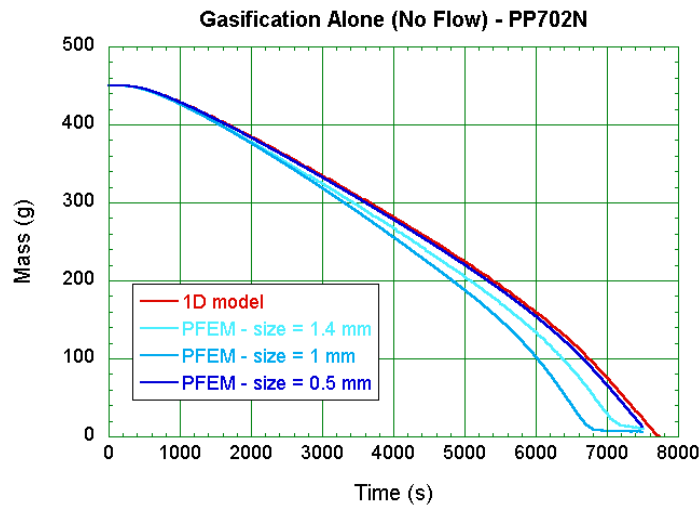
and the velocity at the surface is $dL/dt = W(L, t)$. The initial conditions are $T = T_0$ and $L = L_0$ at time $t = 0$. An adiabatic boundary condition $\rho T / \rho z = 0$ is applied at $z = 0$, and at $z = L(t)$ the boundary condition is

$$-k \frac{\partial T}{\partial z} = \epsilon q_0 + \epsilon s (T^4 - T_0^4) + h_c (T - T_0) \quad , \quad [4]$$

where q_0 is incident heat flux, ϵ is emissivity, s is the Stefan-Boltzmann constant, and h_c is the convective heat transfer coefficient. This 1D model was solved using Mathematica.

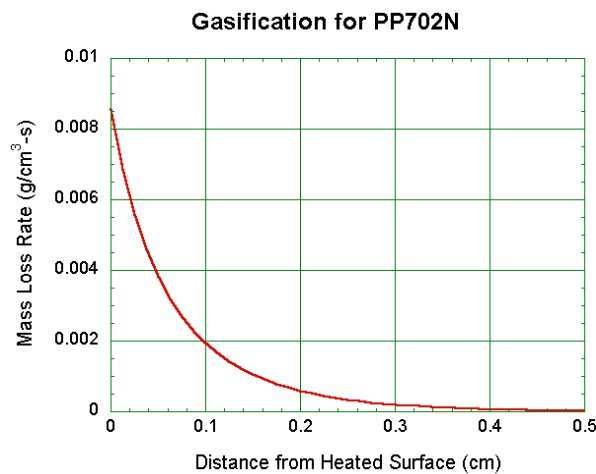
Figure 9 compares the mass as a function of time for the 1D model with the PFEM model using initial particle spacings of 0.5, 1.0, and 1.5 mm. The heat flux to the free surface is 30 kW/m^2 .

Figure 9. Comparison of mass vs. time for PFEM model at three spatial resolutions against 1D gasification model.



There is very close agreement between the PFEM model and the 1D model for an initial particle spacing of 0.5 mm, but the discrepancy for larger spacings is significant. The reason for this is explained by Figure 10, which shows the mass loss rate as a function of distance into the heated surface at time $t = 5000$ s.

Figure 10. Mass loss rate as a function of distance for PP702N.



With the Arrhenius parameters for PP702N, the mass loss rate due to gasification drops to less than one-tenth of the surface value within 2 mm, indicating that a spatial resolution on the order of 0.5 mm is needed in the gasification layer. The mass loss rate is overestimated for larger particle spacings, leading to the more rapid decreases in mass in Figure 9 for sizes of 1 mm or 1.4 mm. Since the high resolution gasification problem took about 19 hours to run, there is a need for higher efficiency in the PFEM code to run a problem containing both gasification and flow with good accuracy. A good solution is adaptive gridding, with new particles continuously fed into the flow layer to maintain high resolution there without wasting resources in the immobile cold region away from the surface.

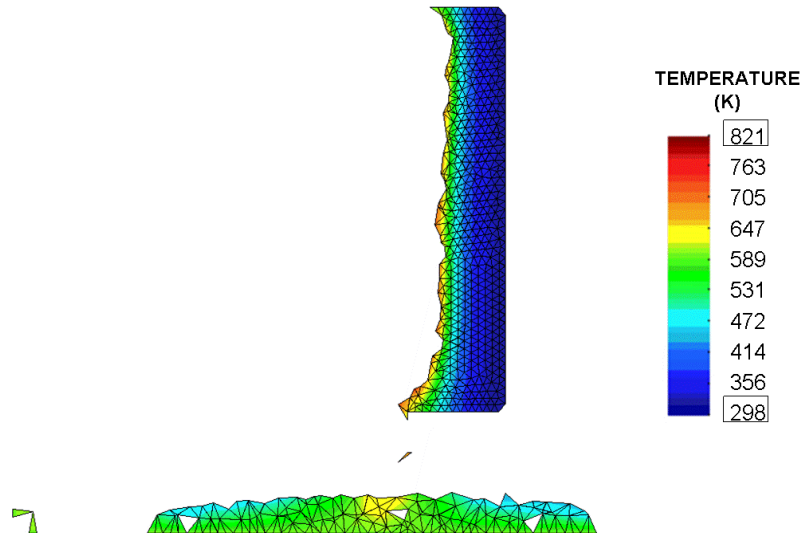
Flow onto catch surface

The addition of a catch pan to capture the dripping polymer melt tests the ability of the PFEM model to recover mass when a particle or set of particles reaches the catch surface. For this problem,

heat flux is only applied to free surfaces above the midpoint between the catch pan and the base of the sample. However, every free surface is subject to radiative and convective heat losses. To keep the melt fluid, the catch pan is set to a temperature of 600 K. The thickness of the sample is reduced to 2.5 cm to achieve results more quickly.

Figure 11 shows the flow into the catch pan at time $t = 600$ s. Directly below the base of the sample where the melt is dripping, the temperature of the melt is higher. On the catch pan away from this point, the top of the melt has cooled to a temperature below the 600 K of the catch pan surface.

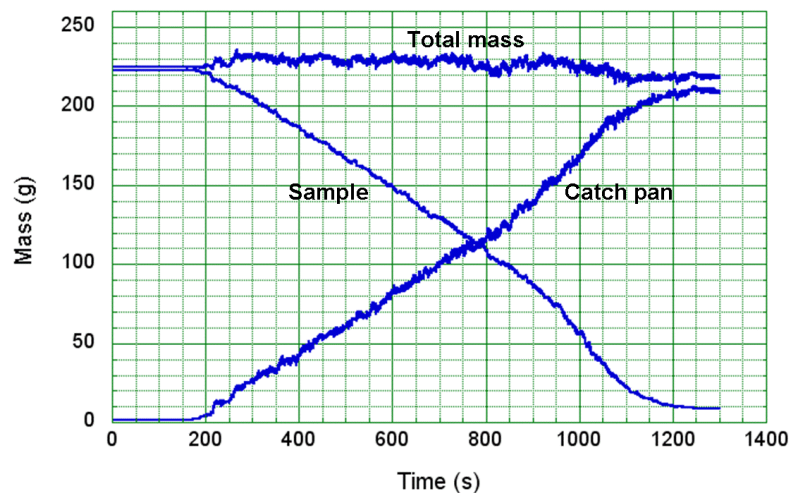
Figure 11. Flow into catch pan at $t = 600$ s.



The melt spreads to either side from the point at which the dripping melt contacts the catch pan.

Figure 12 shows the mass of the sample, the mass of the melt on the catch pan, and their sum. After a heating time of about 170 s, the mass begins to be transferred from the sample to the catch pan. The total mass reflects a conservation of mass within $\pm 5\%$. Note that because of the statistical nature of the PFEM, the total mass at times exceeds 100% of the initial mass.

Figure 12. Mass vs. time for polymer in sample, in catch pan, and total mass.

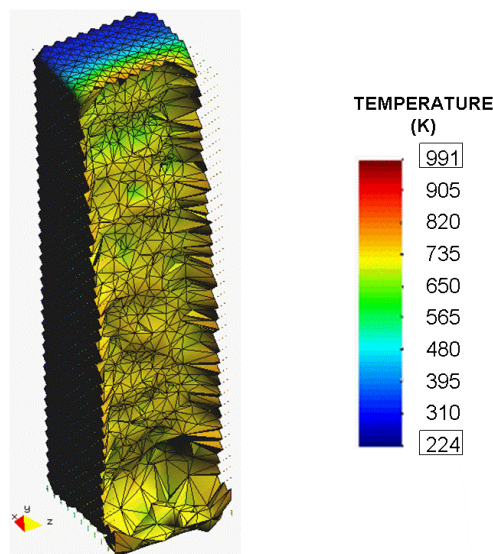


The effects of the material properties and thickness of the catch pan on the spread of polymer melt can easily be studied using this approach, since the PFEM uses particles to represent solids in the same manner as fluids.

Three-dimensional flow from heated sample

To test the ability of the PFEM to solve this type of problem in three dimensions as well as in two, a 3D problem for flow from a heated sample was run. The same boundary conditions are used as in the 2D problem illustrated in Figure 5, but the initial dimensions of the sample are reduced to 10 cm high by 2.5 cm wide by 2.5 cm thick. The initial size of the model is 22475 nodes and 97600 elements, and the runtime for this problem was slightly over a week. The shape of the surface and the temperature field at 450 seconds after heating begins are shown in Figure 13.

Figure 13. Flow from a 3D heated sample at $t = 450$ s.



Note that, for this symmetrical problem, the model could have been halved in size along the vertical axis to give the same results in one-quarter the time.

Edge effects in the 3D model slow the rate of flow along the side walls, resulting in a thicker sample there throughout the melt flow process. This has also been observed in the experiments. Although the resolution for this problem is not fine enough to achieve high accuracy, the qualitative agreement of this 3D model with 2D flow and the ability to carry out this problem in a reasonable amount of time suggest that the PFEM can be used to model complex 3D flow geometries. Improved efficiency is needed to make such calculations routine.

CONCLUSION

The Particle Finite Element Method is shown to track the changes in shape of a thermoplastic solid subjected to a heat source. This is the first step in developing a model to investigate the effects of changing geometry due to melt flow on flame spread.

Most 2D problems took less than a day to run, and a 3D problem showing flow from the heated sample was completed in a little over a week. The addition of adaptive gridding and other measures to improve efficiency will both improve the runtime and enable more accurate results.

ACKNOWLEDGMENT

The authors would like to thank Thomas Ohlemiller for keeping the development of the melt flow model well grounded in experimental evidence.

REFERENCES

- ¹ Zhang, J., Shields, T.J., Silcock, G.W.H., “Effect of melting behaviour on flame spread of thermoplastics”, *Fire & Materials*, Vol. 21, No. 1, Jan – Feb 1997, pp. 1-6.
- ² Fleischmann, C.M. and Hill, G.R., “Burning behaviour of upholstered furniture”, Interflam 2004, Interscience Communications Ltd, London, UK, pp. 907-916.
- ³ Sherratt, J. and Drysdale, D., “The effect of the melt-flow process on the fire behaviour of thermoplastics”, Interflam 2001, Interscience Communications Ltd, London, UK, pp. 149-159.
- ⁴ Butler, K.M., Ohlemiller, T.J., Linteris, G.T., “A Progress Report on Numerical Modeling of Experimental Polymer Melt Flow Behavior”, Interflam 2004, Interscience Communications Ltd, London, UK, pp. 937-948.
- ⁵ Li, S. and Liu, W.K., *Meshfree Particle Methods*, Springer-Verlag Berlin, 2004.
- ⁶ Idelsohn, S.R., Oñate, E., Del Pin, F., “The particle finite element method: a powerful tool to solve incompressible flows with free-surfaces and breaking waves”, *Int. J. Num. Meth. Engng.*, Vol. 61, 2004, pp. 964-989.
- ⁷ Idelsohn, S.R., Oñate, E., Del Pin, F., “A lagrangian meshless finite element method applied to fluid-structure interaction problems”, *Computer and Structures*, Vol. 81, 2003a, pp. 655-671.
- ⁸ Oñate, E., Rojek, J., Chuimenti, M., Idelsohn, S.R., Del Pin, F., Aubry, R., “Advances in stabilized finite element and particle methods for bulk forming processes”, *Comput. Methods Appl. Mech. Engrg.*, Vol. 195, 2006, pp. 6750-6777.
- ⁹ Ohlemiller, T.J., Shields, J.R., Butler, K.M., Collins, B., Seck, M., “Exploring the role of polymer melt viscosity in melt flow and flammability behavior”, *Proceedings of the Fall Conference of the Fire Retardant Chemicals Association*, Oct 2000, pp. 1-28.
- ¹⁰ Edelsbrunner, H. and Mücke, E.P., “Three dimensional alpha shapes”, *ACM Trans. Graphics*, Vol. 13, 1999, pp. 43-72.
- ¹¹ Idelsohn, S.R., Oñate, E., Calvo, N., Del Pin, F., “The meshless finite element method”, *Int. J. Num. Meth. Engng.*, Vol. 58 N. 6, 2003b, pp. 893-912.